Warming does not delay the start of autumnal leaf coloration but slows its progress rate

Nan Jiang, Miaogen Shen, Philippe Ciais, Matteo Campioli, Josep Peñuelas, Christian Körner, Ruyin Cao, Shilong Piao, Licong Liu, Shiping Wang, et al.

Received: 15 December 2021 | Revised: 9 July 2022 | Accepted: 20 July 2022

DOI: 10.1111/geb.13581

Global Ecology and Biogeography | A Journal of Macroecology | WILEY

RESEARCH ARTICLE

Warming does not delay the start of autumnal leaf coloration but slows its progress rate

Nan Jiang[1,2] | Miaogen Shen[2] | Philippe Ciais[3] | Matteo Campioli[4] | Josep Peñuelas[5,6] | Christian Körner[7] | Ruyin Cao[8] | Shilong Piao[1,9] | Licong Liu[2] | Shiping Wang[1] | Eryuan Liang[1] | Nicolas Delpierre[10] | Kamel Soudani[10] | Yuhan Rao[11] | Leonardo Montagnani[12,13] | Lukas Hörtnagl[14] | Eugénie Paul-Limoges[15] | Ranga Myneni[16] | Georg Wohlfahrt[17] | Yongshuo Fu[18] | Ladislav Šigut[19] | Andrej Varlagin[20] | Jin Chen[2] | Yanhong Tang[9] | Wenwu Zhao[2]

[1]State Key Laboratory of Tibetan Plateau Earth System, Resources and Environment (TPESRE), Institute of Tibetan Plateau Research, Chinese Academy of Sciences, Beijing, China

[2]State Key Laboratory of Earth Surface Processes and Resource Ecology, Faculty of Geographical Science, Beijing Normal University, Beijing, China

[3]Laboratoire des Sciences du Climat et de l'Environnement (LSCE), CEA CNRS UVSQ, Gif Sur Yvette, France

[4]Centre of Excellence PLECO (Plants and Ecosystems), Department of Biology, University of Antwerp, Wilrijk, Belgium

[5]CSIC, Global Ecology Unit CREAF-CEAB-UAB, Bellaterra, Spain

[6]CREAF, Cerdanyola del Vallès, Spain

[7]Institute of Botany, University of Basel, Basel, Switzerland

[8]School of Resources and Environment, University of Electronic Science and Technology of China, Chengdu, China

[9]College of Urban and Environmental Sciences, Peking University, Beijing, China

[10]CNRS, AgroParisTech, Ecologie Systématique et Evolution, Université Paris-Saclay, Orsay, France

[11]North Carolina Institute for Climate Studies, North Carolina State University, Asheville, North Carolina, USA

[12]Forest Service, Autonomous Province of Bolzano-Bozen, Bolzano-Bozen, Italy

[13]Faculty of Science and Technology, Free University of Bolzano, Bolzano, Italy

[14]Department of Environmental Systems Science, Institute of Agricultural Sciences, ETH Zurich, Zurich, Switzerland

[15]Department of Geography, University of Zurich, Zurich, Switzerland

[16]Department of Earth and Environment, Boston University, Boston, Massachusetts, USA

[17]Department of Ecology, University of Innsbruck, Innsbruck, Austria

[18]College of Water Sciences, Beijing Normal University, Beijing, China

[19]Department of Matter and Energy Fluxes, Global Change Research Institute of the Czech Academy of Sciences, Brno, Czech Republic

[20]A.N. Severtsov Institute of Ecology and Evolution, Russian Academy of Sciences, Moscow, Russia

Correspondence
Miaogen Shen, State Key Laboratory of Earth Surface Processes and Resource Ecology, Faculty of Geographical Science, Beijing Normal University, Beijing 100875, China.
Email: shen.miaogen@gmail.com

Handling Editor: Stephanie Pau

Abstract

Aim: Initiation of autumnal leaf senescence is crucial for plant overwintering and ecosystem dynamics. Previous studies have focused on the advanced stages of autumnal leaf senescence and reported that climatic warming delayed senescence, despite the fundamental differences among the stages of senescence. However, the timing of onset of leaf coloration (D_{LCO}), the earliest visual sign of senescence, has rarely been studied. Here, we assessed the response of D_{LCO} to temperature.

Location: 30–75° N in the Northern Hemisphere.

Time period: 2000–2018.

Major taxa studied: Deciduous vegetation.

Methods: We retrieved D_{LCO} from high-temporal-resolution satellite data, which were then validated by PhenoCam observations. We investigated the temporal changes in D_{LCO} and the relationship between D_{LCO} and temperature by using satellite and ground observations.

Results: D_{LCO} was not significantly ($p > .05$) delayed between 2000 and 2018 in 94% of the area. D_{LCO} was positively ($p < .05$) correlated with pre-D_{LCO} mean daily minimum temperature (T_{min}) in only 9% of the area, whereas the end of leaf coloration (D_{LCE}) was positively correlated with pre-D_{LCE} mean T_{min} over a larger area (34%). Further analyses showed that warming slowed the progress of leaf coloration. Interestingly, D_{LCO} was less responsive to pre-D_{LCO} mean T_{min} in areas where daylength was longer across the Northern Hemisphere, particularly for woody vegetation.

Main conclusions: The rate of progress of coloration is more sensitive to temperature than its start date, resulting in an extension of the duration of leaf senescence under warming. The dependence of D_{LCO} response to temperature on daylength indicates stronger photoperiodic control on initiation of leaf senescence in areas with longer daylength (i.e., shorter nights), possibly because plants respond to the length of uninterrupted darkness rather than daylength. This study indicates that the onset of leaf coloration was not responsive to climate warming and provides observational evidence of photoperiod control of autumnal leaf senescence at biome and continental scales.

KEYWORDS
autumnal leaf senescence, global warming, leaf coloration onset, Northern Hemisphere, photoperiod

1 | INTRODUCTION

In contrast to the leaves of evergreen conifers, those of northern deciduous plants are not sufficiently tolerant of freezing to survive cold periods and, therefore, are shed before the onset of winter. This autumnal senescence process is controlled by changes in gene expression and metabolic adjustments that include the degradation of macromolecules (e.g., chlorophyll), a decrease in photosynthesis and, importantly, the recycling and re-allocation of nutrients (Gan & Amasino, 1997; Thomas & Stoddart, 1980). In parallel to leaf senescence, carbon sink activity ceases progressively, and plants switch to nutrient recovery and resorption processes (Estiarte & Peñuelas, 2015; Keskitalo et al., 2005). Without timely leaf senescence and abscission, early frost would reduce nutrient resorption, leading to a loss of leaf resources. Changes in the timing of key steps of leaf senescence extensively influence ecosystem structure and functions, such as vegetation activity, trophic interaction, carbon and nutrient cycling, land–atmosphere moisture and energy fluxes (Keenan et al., 2014; Morisette et al., 2009), which could further affect the climate system (Peñuelas et al., 2009; Richardson et al., 2013).

Senescence starts as a cryptic phenological process before any visible symptoms become apparent (Körner & Basler, 2010). The timing of the start of the leaf coloration following senescence varies, depending on the rate of the senescence process, which is related to environmental conditions (e.g., temperature) (Fracheboud et al., 2009). Hence, the process of autumnal leaf senescence has two phases (Figure 1a): (1) a visually indistinguishable ontogenetic stage that precedes (2) a visible change in leaf colour (Tang et al., 2016). The timings of the middle and end of leaf coloration are the focus of *in situ* phenological observations and have been the main concern of most autumnal phenological studies to date.

Satellite and ground-based observations indicate that climate warming in the last several decades has substantially advanced the onset of spring green-up and the peak of the growing season, and it has slightly delayed the timing of the end of leaf coloration [D_{LCE}, the time when the normalized difference vegetation index (NDVI) decreases by 50% of its annual amplitude in the second half of a year in satellite-based studies (Ganguly et al., 2010; Lukasová et al., 2019; Melaas et al., 2013; Nagai et al., 2010; White et al., 1997; Yu et al., 2010)] in the Northern Hemisphere (Figure 1b) (Fu et al., 2015, 2019; Gill et al., 2015; Jeganathan et al., 2014; Menzel et al., 2020; Xu et al., 2016). In addition to temperature, an increase in precipitation also delays D_{LCE} in temperate dry grasslands in the northern middle latitudes (Liu et al., 2016). Besides these abiotic factors, temporal changes in D_{LCE} are also associated with the onset of green-up in some temperate tree species (Keenan & Richardson, 2015) and in boreal ecosystems (Liu et al., 2016). In contrast to D_{LCE}, the timing of onset of leaf coloration (D_{LCO}; Figure 1b) has been studied inadequately. In

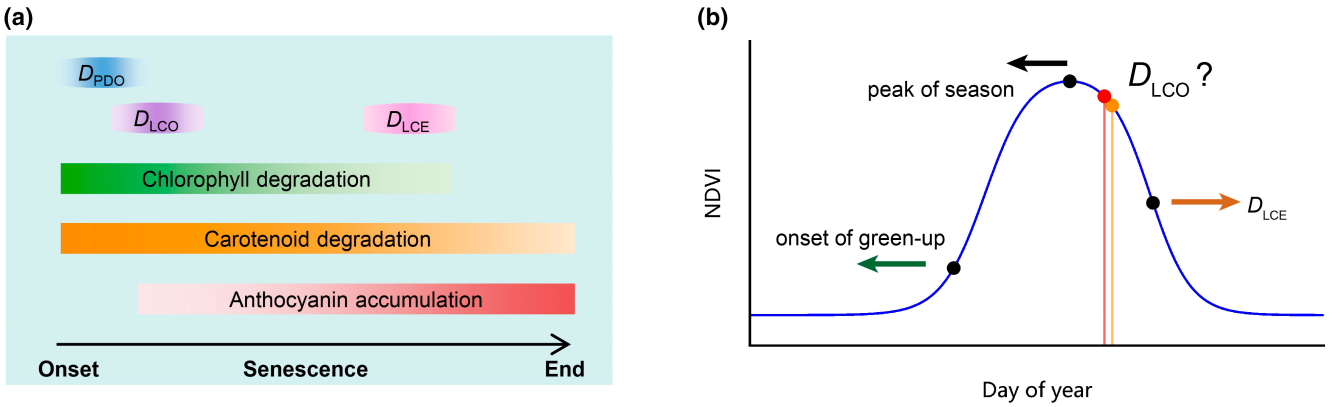

FIGURE 1 Conceptual graphs illustrating (a) the developmental processes in pigments during leaf senescence that are related to photosynthetic capacity and leaf colour; and (b) phenological changes retrieved from the normalized difference vegetation index (NDVI) in the last few decades. In (a), D_{PDO} and D_{LCO} are the timings of the onsets of the decrease in maximum canopy photosynthetic capacity and leaf coloration in autumn, respectively; D_{LCE} is the timing of the end of leaf coloration. In (b), the onset of green-up corresponds to a 20% increase in NDVI in spring, the peak of the season corresponds to the maximum NDVI, and D_{LCE} corresponds to a 50% decrease in NDVI in autumn. D_{LCO} was defined by two methods, corresponding to a 10% decrease in NDVI (orange point) and the inflection point at which NDVI begins to decline (red point), respectively (for details, see Section 2). The leftward and rightward arrows indicate advances of onset of green-up and peak of season and delay of D_{LCE}, respectively, over the past few decades. The question mark indicates a research gap regarding temporal changes in D_{LCO} and their drivers.

particular, it is not known whether D_{LCO} is sensitive to climate and whether it has been responsive to recent climate change. D_{LCO} is of key importance because it indicates when leaf senescence becomes detectable from NDVI and its progress accelerates (Figure 1b). As shown by experiments on young trees, some temperate and boreal woody species use the shortening of the photoperiod as a signal for the onset of leaf senescence (Supporting Information Table S1), but many *in situ* and satellite observations indicate that increased temperature induces delays in the advanced stages of senescence, such as D_{LCE} (Delpierre et al., 2009; Estrella & Menzel, 2006; Ge et al., 2015; Gill et al., 2015; Jeong et al., 2011; Liu et al., 2016).

A dominant photoperiodic control of early senescence implies that D_{LCO} should not be delayed, even if the temperature increases, because its timing is controlled only by daylength (hypothesis 1). Moreover, because D_{LCE} delays with warmer temperature, we may further hypothesize that earlier stages of leaf senescence are less sensitive to temperature than are more advanced stages and expect an extension of the period between D_{LCE} and D_{LCO} under warming. In contrast, without photoperiodic control, shifts in D_{LCO} are expected in the case of climatic warming (hypothesis 2). Alternatively, if D_{LCO} is influenced by both photoperiod and temperature, the relationships between D_{LCO} and temperature should vary among different areas, because the strength of the photoperiod signal varies (hypothesis 3).

To test these hypotheses, we initially investigated the temporal changes in D_{LCO} and the interannual relationships between D_{LCO} and pre-D_{LCO} T_{min} (the mean of monthly average daily minimum temperature for an optimized period preceding D_{LCO}) for northern vegetation (30–75° N, with cropland pixels excluded) during the period 2000–2018. We then examined whether the timings of earlier stages of leaf coloration are less responsive to temperature and show fewer delays and assessed the impacts of temperature on the progress of leaf coloration. Given that only a few *in situ* observational programs or networks have monitored D_{LCO}, we determined D_{LCO} from a 5-day composite time series of the NDVI derived from daily surface spectral reflectance (MOD09CMG) at a spatial resolution of .05°, provided by the spaceborne Moderate Resolution Imaging Spectroradiometer (MODIS) (Vermote, 2015). To complement the NDVI data, we also used 332 time series of D_{LCO} observed by professional observers according to standard observation guidelines (China Meteorological Administration, 1993) in the field in China (Supporting Information Figure S1a; Table S2) and the timing of onset of autumnal decline in maximum canopy photosynthetic capacity (D_{PDO}) derived from eddy covariance CO_2 flux observations (Gu et al., 2009; Shen, Tang, et al., 2014) at 36 sites from within the FLUXNET2015 dataset (Pastorello et al., 2017) (Supporting Information Figure S1b; Table S3).

2 | MATERIALS AND METHODS

2.1 | Estimating timings of stages of leaf coloration from satellite observations of NDVI time series

2.1.1 | Dataset and preprocessing

The NDVI is a proxy for vegetation greenness and has been widely used for phenological studies at large spatial scales (Buitenwerf et al., 2015; Gao et al., 2019; Keenan et al., 2014; Myneni et al., 1997; Wu et al., 2018). NDVI has also been proved capable of detecting the onset of leaf coloration (Mariën et al., 2019; Soudani et al., 2012, 2021; Yang et al., 2014; Zhao et al., 2020). Previous studies have usually used half-month/16-day composite NDVI time series to retrieve phenological metrics. However, because the duration of leaf coloration could be as short as 4 weeks in some areas (Ye & Zhang, 2021), NDVI time-series data with higher temporal resolution are required.

We estimated phenological metrics (i.e., the timings of the onset and the advanced stages of leaf coloration and the onset of green-up) for 2000–2018 from a 5-day composite NDVI time series produced from the MODIS reflectance product (MOD09CMG Collection 6, available at: https://ladsweb.modaps.eosdis.nasa.gov, accessed on 29 January 2019) (Vermote, 2015). MOD09CMG provides an estimate of daily surface spectral reflectance at a spatial resolution of .05°. The quality of the daily surface reflectance data from MOD09CMG is unsatisfactory owing to cloud and snow contamination (Vermote, 2015); therefore, we used the 5-day maximum value composite approach (Zhang, 2015), combined with a Savitzky–Golay filter (Cao et al., 2018), to produce a high-quality NDVI time series before determining D_{LCO}. Initially, NDVI values that were lower than the uncontaminated winter (December–February) mean NDVI were replaced by the latter (Beck et al., 2006; Zhang et al., 2007). After that, cloud-contaminated and irregularly high and low NDVI values were identified and reconstructed by using a Savitzky–Golay filter (Cao et al., 2018). Details for preparation of the high-quality NDVI time series are given in the Supporting Information (Section 1 of the Supplementary Methods).

We focused on natural vegetation by excluding pixels dominated by cropland, artificial surfaces, permanent snow or ice, and water bodies, on the basis of the MODIS land-cover map (MCD12C1 Version 6, available at: https://ladsweb.modaps.eosdis.nasa.gov, accessed on 20 August 2018) (Friedl & Sulla-Menashe, 2015) for the middle year of the time series (2009). Some pixels were also excluded from analysis because of sparse vegetation coverage, weak seasonality, or NDVI peaking in October–April. We adopted three criteria for pixel inclusion: mean annual NDVI must be >.10 (Jeong et al., 2011); NDVI should peak between May and September in the multiyear mean NDVI time series (Shen et al., 2020); and mean NDVI for July and August must be >1.15 times the mean NDVI for December and for January–February in every year (Shen, Zhang, et al., 2014).

2.1.2 | Estimation of timings of leaf coloration

Two methods can generally be used to estimate the parameters of vegetation phenology (Chen et al., 2016; Shang et al., 2017), including D_{LCO} from annual NDVI profiles. One is based on thresholds (White et al., 1997), whereas the other is based on inflection points (Zhang et al., 2003). We applied the threshold-based method by initially using a generalized sigmoid function to fit the NDVI annual profile [Equation (7) in the paper by Klosterman et al., 2014] and then determining D_{LCO} as the first date when NDVI decreased by 10% of its annual amplitude in the descending period (Leblans et al., 2017; Richardson et al., 2018). Although a smaller decrease in NDVI corresponds to an earlier stage of leaf coloration, consideration of it would introduce more uncertainty. We also determined D_{LCO} by using the algorithm based on inflection point. In this method, D_{LCO} was defined as the date when the rate of change of the curvature of a double logistic function (Beck et al., 2006; Elmore et al., 2012) fitted to the NDVI time series reached its first local minimum in the descending period (Zhang et al., 2003). Theoretically, the D_{LCO} defined by the inflection method is close to the date when NDVI decreases by *c*. 9% of its annual magnitude (Shang et al., 2017).

The advanced stages of leaf coloration were determined as the dates when NDVI decreases by 20, 30, 40 and 50% (corresponding to the timing of the end of leaf coloration, D_{LCE}) of its annual amplitude, respectively. In addition, given that in a few studies (Berman et al., 2020; Ren et al., 2017) the end of leaf coloration was defined as the dates when NDVI drops by 60 or 90% of its annual amplitude, we also included these definitions in analysis. We defined the timing of the onset of green-up as the date when NDVI increased by 20% (Yu et al., 2010).

2.1.3 | Evaluation of satellite D_{LCO} using PhenoCam

It is unreasonable to validate the satellite-derived D_{LCO} by comparing it with the D_{LCO} of a few plant individuals from ground observation, because of mismatch in spatial coverage, different definitions of phenological metrics, and the spatial heterogeneity in phenological phases among individuals for a pixel. Fortunately, pairs of field observations of NDVI and leaf coloration showed good consistency between the start of NDVI decrease and the onset of leaf coloration (Soudani et al., 2012, 2021). Moreover, the comparison between the start of autumn from satellite-observed NDVI and field observations of leaf coloration onset for the entire area covered by the pixel also showed little difference between them (Zhao et al., 2020). Those studies suggest that NDVI is capable of detecting the onset of leaf coloration if the observed leaves or individuals are identical between ground and satellite observations. However, there are very limited pairs of compatible observations of NDVI and leaf coloration that can be used for validation.

Considering the high capability of PhenoCam in capturing the variations in leaf coloration onset at the landscape scale (Klosterman et al., 2014; Klosterman & Richardson, 2017; Nezval et al., 2020; Wingate et al., 2015), we used the PhenoCam dataset v.2.0 (Richardson et al., 2018; Seyednasrollah, Young, Hufkens, Milliman, Friedl, Frolking, & Richardson, 2019; Seyednasrollah, Young, Hufkens, Milliman, Friedl, Frolking, Richardson, Abraha, et al., 2019) to assess the relationships between satellite-derived D_{LCO} and the D_{LCO} derived from time series of the green chromatic coordinate (GCC) and vegetation contrast index (VCI) observed by PhenoCam. The GCC and VCI were determined from the digital numbers (*DN*) in red (R), green (G) and blue (B) channels. Specifically, GCC and VCI were calculated as $DN_G/(DN_R+DN_G+DN_B)$ and $DN_G/(DN_R+DN_B)$, respectively. Details for the determinations of D_{LCO} from time series of GCC and VCI are given in the Supporting Information (Section 2 of the Supplementary Methods).

2.2 | D_{LCO} from *in situ* phenological observations

D_{LCO} was extracted at the species level from datasets of *in situ* phenological observations in China provided by the Chinese Academy of

Sciences (CAS). The CAS dataset uses the date of first leaf colouring as D_{LCO}. For a given species at a given site, the date of first leaf colouring was identified as the day when the first batch (*c*. 5%) of leaves on more than half of three to five marked individuals started to change colour (China Meteorological Administration, 1993). The *in situ* phenological observations were performed visually according to standard observation guidelines (China Meteorological Administration, 1993) every other day by professional observers trained well by CAS. The CAS dataset is available from National Earth System Science Data Sharing Infrastructure, National Science and Technology Infrastructure of China (http://www.geodata.cn, accessed on 25 July 2018).

2.3 | D_{PDO} estimated from maximum canopy photosynthetic capacity

The timing of the onset of the decrease in maximum canopy photosynthetic capacity in autumn (as day of year, D_{PDO}) is defined as the date when the capacity decreases by 10% of its annual amplitude after the data have been fitted to a generalized sigmoid function [Equation (7) in the paper by Klosterman et al., 2014]. The capacity was calculated from half-hourly or hourly gross primary productivity (GPP_NT_CUT_MEAN) based on eddy covariance measurements in the FLUXNET2015 dataset (http://fluxnet.fluxdata.org/data/fluxnet2015-dataset/, accessed on 10 March 2018) (Pastorello et al., 2017). We followed the procedure of Shen, Tang et al. (2014) to estimate daily canopy photosynthetic capacity, except that the parameters in the rectangular hyperbolic function were estimated by using half-hourly/hourly gross primary productivity and incident short-wave radiation calculated by using 15-day moving windows throughout a year. We used data from the sites in non-Mediterranean (Köppen–Geiger climate classification) and non-cultivated (International Geosphere–Biosphere Programme classification) regions at middle and high northern latitudes (30–75° N). In a similar way to the pixel exclusion process that was applied to the satellite retrievals, we discarded sites where weak seasonality (i.e., the mean maximum canopy photosynthesis for June–August was <1.15 times that for December or for January and February) was detected in any year and sites where capacity did not peak in May–September.

2.4 | Analyses

2.4.1 | Temporal changes

Temporal changes of D_{LCO} over the study period were assessed using temporal trends in D_{LCO}, which were quantified as the slopes of linear regressions between D_{LCO} and year by using ordinary least squares regression (OLSR) and *t* tests. To complement the temporal changes assessed by using OLSR, a nonparametric approach (the Theil–Sen estimator and Mann–Kendall test; Sen, 1968; Theil, 1992) was also used to calculate the trends in D_{LCO}. Temporal changes of timings of advanced stages of leaf coloration were assessed in the same way.

The temporal trend was calculated for each time series for the ground-based observations and for each pixel for the satellite observations. We focused only on the temporal trends for the pixels and time series of *in situ* phenological observations with a multiyear mean of D_{LCO} occurring after the summer solstice. Phenological records were not available for some of the years of the time series for calculating more trends, because the time series might have had missing values owing to a lack of observation. However, the time series used for the regressions contained ≥10 years of observational records and at least one record for any 3 years consecutively. If two or more parts of the time series met these criteria, the most recent part was used.

2.4.2 | Partial correlation between D_{LCO} and temperature or precipitation

T_{min} has long been recognized as the indicator of the thermal condition that induces autumnal leaf coloration (Tang et al., 2016), and the duration of the period preceding D_{LCO} in which T_{min} has the largest influence on D_{LCO} could vary among different locations because of differential vegetation characteristics and climate conditions (Gao et al., 2019; Jeong et al., 2011; Matsumoto et al., 2003; Wu et al., 2018). In addition, precipitation might also regulate leaf coloration in dry climates (Liu et al., 2016). Initially, we determined the duration of this period preceding D_{LCO} (referred to as the pre-D_{LCO} period). Taking satellite-derived D_{LCO}, for example, we investigated the impacts of temperature on the D_{LCO} by calculating the partial correlation coefficient (R_{TN}) values between D_{LCO} and the mean of the monthly average daily minimum temperature (T_{min}) for the pre-D_{LCO} period, with concurrent total precipitation as the control variable for 2000–2018. The pre-D_{LCO} period for T_{min} (Supporting Information Figure S2) was defined as the period preceding the multiyear mean D_{LCO} for which T_{min} had the strongest interannual partial correlation with D_{LCO}, with concurrent total precipitation as a control variable (Jeong et al., 2011; Wu et al., 2018). In detail, we first determined several candidate periods that ended at the multiyear mean D_{LCO} and had a duration starting from 1 month, with a step of 1 month. For each of the candidate periods, we calculated the partial correlation coefficient between D_{LCO} and mean T_{min} in each of these periods, then selected the candidate with the highest absolute value of correlation coefficient. If the multiyear mean D_{LCO} was in the first half of a month, then the pre-D_{LCO} period ended at the month preceding the multiyear mean D_{LCO}. Otherwise, the pre-D_{LCO} period ended at the month of the multiyear mean D_{LCO}. The impacts of T_{min} on the advanced stages of leaf coloration were investigated in a similar manner. A few studies have suggested that the date of onset of green-up might affect leaf coloration through carry-over effects (Cong et al., 2017; Fu et al., 2014; Keenan & Richardson, 2015; Liu et al., 2016); therefore, we also considered the case in which the onset of green-up was included as an extra control variable in the partial correlation between D_{LCO} and T_{min}. The pre-D_{LCO} period for precipitation and the impacts of precipitation on D_{LCO} were assessed in a similar manner.

The data for T_{min} and precipitation were extracted from the Climatic Research Unit (CRU) Time-Series (TS) 4.03 dataset (http://data.ceda.ac.uk, accessed on 11 June 2019), which provided monthly data at a spatial resolution of .5°×.5° until 2018. It should be noted that T_{min} in the dataset is an approximation of the mean of daily minimum temperature for a calendar month, which is calculated arithmetically from the gridded monthly mean temperature and the diurnal temperature range (Harris et al., 2014) and does not exactly reflect the interannual variations in the absolute minimum temperature (Körner & Hiltbrunner, 2018) experienced by plants before D_{LCO}. The CRU data were resampled at .05°×.05° by replication to match the D_{LCO} data.

Complementary to the pre-D_{LCO} period in which T_{min} had the strongest interannual partial correlation with D_{LCO}, we also used fixed durations (1 month and 15 days preceding multiyear mean D_{LCO}, respectively) as the pre-D_{LCO} periods. We calculated the partial correlation between D_{LCO} and pre-D_{LCO} T_{min}, with concurrent total precipitation as the control variable. Moreover, we investigated the partial correlation coefficient between D_{LCO} and the lowest T_{min} during the 15 days before the multiyear mean D_{LCO}, with the concurrent mean T_{min} (mean of the remaining 14 T_{min} values after removal of the lowest T_{min} during the period) and total precipitation as control variables. Note that when the pre-D_{LCO} period was defined as the 15 days preceding D_{LCO} and when we analysed the relationship between the lowest T_{min} and D_{LCO}, daily T_{min} and precipitation were extracted from the CRU-NCEP dataset (v.7.2, available at: https://vesg.ipsl.upmc.fr, assessed on 10 January 2019), which provides 6-hourly data at a spatial resolution of .5°×.5° until 2016 (Viovy, 2018). The CRU-NCEP v.7.2 is a combination of two datasets: the CRU TS 3.2 .5°×.5° monthly data covering the period 1901–2002 and the NCEP re-analysis 2.5°×2.5° 6-hourly data covering the period 1948–2016. We determined daily T_{min} as the minimum value of the four 6-hourly minimum temperature values for each day. The CRU-NCEP data were resampled at .05°×.05° by replication to match the D_{LCO} data.

We also investigated the impact of T_{min} and precipitation on D_{LCO} from ground-based observations in China and on D_{PDO} from eddy-covariance sites as complementary to satellite-derived D_{LCO}. Climatic data for *in situ* observations in China were extracted from the "Daily Surface Climate Variables of China" catalogue (a dataset named SURF_CLI_CHN_MUL_DAY_V3.0), which includes daily climate data for 2,474 sites in China from January 1951 to July 2014, provided by the Chinese Meteorological Administration. The distance between phenological and meteorological stations was <25 km. Climatic data for D_{PDO} were calculated from the half-hourly temperature dataset provided by FLUXNET2015.

2.4.3 | Relationships between the progress of leaf coloration and temperature

The impacts of temperature on the progress of leaf coloration were assessed in four ways.

First, we calculated the partial correlation coefficient between each of the timings of different stages in leaf coloration (determined as NDVI decreases by 20, 30, 40, 50, 60 and 90%) and preceding T_{min} using the approach described in Section 2.4.2. We then compared the percentage of area corresponding to the partial correlation coefficient among the different timings.

Second, the difference in temperature sensitivity between the D_{LCE} and D_{LCO} was used to assess the differential responses to T_{min} between D_{LCE} and D_{LCO}. The temperature sensitivity of D_{LCO} was defined as the coefficient for pre-D_{LCO} T_{min} in a linear regression in which D_{LCO} was set as the dependent variable, and pre-D_{LCO} T_{min} and pre-D_{LCO} total precipitation were independent variables. The temperature sensitivity of D_{LCE} was calculated in a similar manner. See Section 2.4.2 for the details of the determination of pre-D_{LCO} (or pre-D_{LCE}) T_{min} and total precipitation.

Third, the temperature sensitivity of the duration of leaf coloration was used to assess the impact of temperature on the duration of leaf coloration. The duration of leaf coloration was defined as the difference between D_{LCE} and D_{LCO}. Its temperature sensitivity was estimated as the coefficient for mean T_{min} in the linear regression in which the duration was set as the dependent variable and the mean T_{min} and total precipitation in the period between D_{LCE} and D_{LCO} were independent variables.

Fourth, the temperature sensitivity of the speed of leaf coloration was used to assess the impact of temperature on the speed of leaf coloration within a season. The speed of leaf coloration within a season was defined as the normalized decreasing speed of NDVI between D_{LCE} and D_{LCO}, calculated as $-(NDVI_{DLCE} - NDVI_{DLCO})/(D_{LCE} - D_{LCO})/AMP_{NDVI}$, where AMP_{NDVI} is the annual amplitude of NDVI for a given pixel and given year. The temperature sensitivity of the speed of leaf coloration was then calculated as the coefficient for mean T_{min} when regressing the speed of leaf coloration against mean T_{min} and total precipitation between D_{LCE} and D_{LCO}. Here, T_{min} and precipitation were extracted from the CRU TS 4.03 monthly data.

2.4.4 | Dependence of D_{LCO} on daylength

Previous experimental findings suggest that daylength is a signal for the start of autumn leaf senescence (Supporting Information Table S1), indicating a photoperiodic control of D_{LCO}. However, it is difficult to assess the role of daylength by using interannual correlations between D_{LCO} and daylength in natural conditions, because the daylength on a given date does not vary among years. Alternatively, because control of photoperiod on autumn leaf phenology might vary with daylength across different regions (Howe et al., 1995; Pau et al., 2011; Paus et al., 1986; Saikkonen et al., 2012), we examined the variabilities in the correlation between D_{LCO} and T_{min} and in temporal changes in D_{LCO} against the spatial gradient of daylength to explore the dependence of D_{LCO} on daylength. Meanwhile, the spatial variations in the response of autumn leaf phenology to temperature might be associated with local background temperature conditions (Ford et al., 2017; Zohner et al., 2016). Hence, the spatial variations in background

temperature should be minimized when assessing the dependence of D_{LCO} on daylength. To do this, we first calculated the daylength for each pixel at the date of multiyear mean D_{LCO} over the period 2000–2018 and the mean T_{min} of the period before multiyear mean D_{LCO}. The period before multiyear mean D_{LCO} was the month preceding the multiyear mean D_{LCO} if the multiyear mean D_{LCO} was in the first half of a month; otherwise, the period was the month of the multiyear mean D_{LCO}. Next, for each cell of 1.5-h daylength and 4 °C mean T_{min} in the space of the daylength and mean T_{min} (for a graphical illustration, see Figure 5), we calculated the percentage of area with significant ($p < .05$, t test) D_{LCO} delays, the average of positive correlation, and the percentage of area with a positive correlation between D_{LCO} and T_{min} (or precipitation).

In addition, there is more experimental evidence of photoperiodic control on the onset of leaf senescence for woody plants than for herbaceous plants (Supporting Information Table S1), indicating that woody and herbaceous vegetation might respond to photoperiod in different ways. Therefore, the above exploration was also performed separately for woody and herbaceous vegetation. The woody and herbaceous vegetation were merged from Classes 1–6 and Class 10, respectively, in the MODIS land-cover product (MCD12C1, v.6) for 2009 (Friedl & Sulla-Menashe, 2015).

2.4.5 | Possible effect of summer NDVI

In some deciduous forests, NDVI can decline in early summer (i.e., late May–July) before leaf coloration, and this might potentially interfere to some extent with the determination of D_{LCO} (Elmore et al., 2012) and its relationship with temperature. To address this, for the pixels classified as deciduous broadleaf forest in the MODIS land-cover product (Friedl & Sulla-Menashe, 2015), we redefined D_{LCO} considering the possible effect of summer NDVI decline on D_{LCO} and then re-analysed the trends in D_{LCO} and the relationship between D_{LCO} and temperature as described in Sections 2.4.1 and 2.4.2.

For the sake of robustness, the possible effect of summer NDVI decline on D_{LCO} was considered in three different ways. First, we used a modified double logistic model that considers early summer NDVI decline (Elmore et al., 2012) to fit the NDVI time series instead of the original double logistic function for the pixels classified as deciduous broadleaf forest. D_{LCO} was then determined as the date when the rate of change of the curvature of a double logistic function fitted to the NDVI time series reached its first local minimum in the descending period. Second, D_{LCO} was defined as the date when NDVI decreased by 10% of its annual amplitude from 1 August. The maximum value used to determine the annual amplitude was the mean value of the upper quartile of the fitted NDVI values in August. Third, D_{LCO} was defined as the date when NDVI decreased by 10% of its annual amplitude from 16 August. The maximum value used to determine the annual amplitude was the mean value of the upper quartile of the fitted NDVI values in the second half of August.

2.4.6 | Possible cold events before D_{LCO} (or D_{PDO})

A sudden drop of night-time temperature to the freezing point can induce leaf coloration in a few days (Körner, 2007), and this might interfere with our partial correlation analysis between D_{LCO} (or D_{PDO}) and temperature. Hence, we re-examined the temporal changes in D_{LCO} and the correlation between D_{LCO} and temperature as described in Sections 2.4.1 and 2.4.2, after excluding possible cold events estimated using an empirical approach as follows (taking satellite-derived D_{LCO} as an example).

First, we determined the T_{min} threshold below which there could potentially be a cold event for each pixel. Given that a cold event that induces rapid leaf senescence should happen 1–5 days before D_{LCO}, the lowest T_{min} during the 6–35 days before D_{LCO} for all years was set as the T_{min} threshold. A temperature higher than such a threshold will not induce a cold event. For vegetation in middle and high latitudes, a temperature higher than freezing (0°C) does not cause frost damage (Körner, 2021; Lenz et al., 2013; Sakai & Larcher, 1987; Taschler & Neuner, 2004). Therefore, if the lowest T_{min} was >0°C, the T_{min} threshold was set to 0°C.

Second, for a given pixel, a year was determined as a candidate cold event year if the lowest T_{min} in the period 1–5 days before D_{LCO} was lower than the above-mentioned T_{min} threshold. Then, from the years in which there was no candidate cold event, we determined the latest D_{LCO} that was not caused by a cold event for that pixel.

Finally, a D_{LCO} was recognized as possibly being caused by a cold event if it was in the candidate cold event years and also earlier than the latest D_{LCO} that was not caused by a cold event. For a D_{LCO} (referred to as D'_{LCO}) from the candidate cold event years and later than the latest D_{LCO} that was not caused by a cold event, it (D'_{LCO}) would be recognized as a D_{LCO} possibly caused by a cold event if one of the following two conditions was met: (1) the decreasing rate of T_{min} in the period 1–5 days before D'_{LCO} was faster than the maximum decreasing rate of T_{min} among the years in which there was no candidate cold event; or (2) the decrease (absolute value) in T_{min} in the period 1–5 days before D'_{LCO} was greater than the maximum decrease in T_{min} among the years with no candidate cold event. Here, for a given year, the decreasing rate of T_{min} in the period 1–5 days before D_{LCO} (or D'_{LCO}) was calculated as the minimum of the slopes of T_{min} against calendar date. A slope of T_{min} against calendar date was calculated as $[T_{min}(\text{time2}) - T_{min}(\text{time1})]/(\text{time2} - \text{time1})$, where time2 = $D_{LCO} - 1$, $D_{LCO} - 2$, $D_{LCO} - 3$, $D_{LCO} - 4$ or $D_{LCO} - 5$ and time1 = $D_{LCO} - 2$, $D_{LCO} - 3$, $D_{LCO} - 4$ or $D_{LCO} - 5$, and time2 is later than time1. The decrease in T_{min} in the period 1–5 days before D_{LCO} (or D'_{LCO}) for a given year was the maximum value of magnitudes of $[T_{min}(\text{time2}) - T_{min}(\text{time1})]$.

This empirical approach might have overestimated the number of years with cold events before D_{LCO} (hereafter, these identified events are referred to as possible cold events), but our objective here was to exclude as many cold events as possible, then to examine whether the main findings of our study were caused by cold events. In addition, under clear skies, the temperature of the canopy surface could be lower than the air temperature; therefore, we also

determined the possible cold events by using 2°C as the T_{min} threshold (Körner, 2021).

Here, the daily T_{min} used to determine possible cold events for satellite-derived D_{LCO} was extracted from the CRU-NCEP v.7.2 dataset. Daily T_{min} for ground-based observations in China was derived from the nearest meteorological station (<25 km), provided by the Chinese Meteorological Administration. Daily T_{min} for D_{PDO} was calculated from the half-hourly temperature dataset provided by FLUXNET2015.

3 | RESULTS

3.1 | Comparison of satellite D_{LCO} with PhenoCam D_{LCO}

The satellite D_{LCO} explained >80% of the variations in PhenoCam-derived D_{LCO} (n = 378 and 377 for GCC and VCI, respectively; Figure 2). The differences between the satellite-derived D_{LCO} and the PhenoCam-derived D_{LCO} are caused by the mismatch between the annual NDVI and GCC (or VCI) trajectories owing to the difference in spatial coverage between the PhenoCam and satellite pixels in the case of phenologically heterogeneous land surface (see Supporting Information Supplementary Methods Section 2).

3.2 | Proportion of possible cold events before D_{LCO} (or D_{PDO})

Possible cold events occurred before D_{LCO} or D_{PDO} in very small fractions of pixel-years/site-years with phenological data (1.6, 1.7 and .6% for satellite-derived D_{LCO}, ground-based observations in China, and D_{PDO} from eddy-covariance sites, respectively; Table 1). The proportion of years possibly affected by cold events was slightly higher when using the method based on a temperature threshold of 2°C than that of 0°C.

3.3 | Temporal trends in D_{LCO} and the advanced stages of leaf coloration

D_{LCO} was not significantly delayed in 94% of the area during the study period, as assessed by OLSR. The few pixels with a significant delay trend (6%; $p < .05$, t test) were scattered across the Northern Hemisphere (Figure 3a). Excluding years with possible cold events before D_{LCO} produced similar results (Supporting Information Figure S3; Table S4). The Theil–Sen estimator generated results supporting the lack of changes in D_{LCO} (no significant delay in 96% of the area; $p < .05$, Mann–Kendall test; Supporting Information Figure S4a; Table S5). When we defined D_{LCO} as the inflection point at which NDVI begins to decline, we obtained similar results (Supporting Information Figure S4b,c). Considering early summer NDVI decline produced similar results (Supporting Information Figures S5–S7).

Complementary to satellite-derived D_{LCO}, we also examined the temporal changes of D_{LCO} by using ground-based leaf coloration data from China. D_{LCO} was not significantly delayed for 90 and 94% of the 332 time series as shown by OLSR (Figure 3b) and the Theil–Sen method (Supporting Information Table S5), respectively. Similar results were produced when possible cold events were excluded (Supporting Information Table S4).

The timings of earlier stages of leaf coloration exhibited delaying trends in fewer areas. The leaf coloration stages determined as the dates when NDVI decreases by 50% (i.e., D_{LCE}), 40, 30, 20 and 10% (i.e., D_{LCO}) were significantly ($p < .05$, t test) delayed for 14, 14, 12, 9 and 6% of the area, respectively (Supporting Information Figure S8).

3.4 | Correlation between D_{LCO} and temperature or precipitation

D_{LCO} was not consistently correlated with pre-D_{LCO} T_{min}, with only 9% of the area in scattered pixels showing a significant positive correlation and 5% showing a significant negative correlation (Figure 4a). D_{LCO} was positively correlated with pre-D_{LCO} total precipitation in

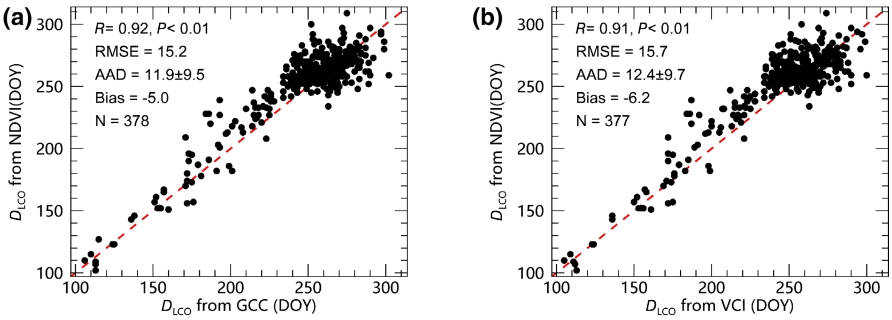

FIGURE 2 Comparison between satellite timing of the onset of leaf coloration in autumn (D_{LCO}) and PhenoCam-derived D_{LCO}. The PhenoCam-derived D_{LCO} was determined from the green chromatic coordinate (GCC; a) and vegetation contrast index (VCI; b), respectively. AAD = average absolute difference; bias is defined as the difference between the mean of satellite-derived D_{LCO} and the mean of PhenoCam-derived D_{LCO}, and negative bias means that the PhenoCam-derived D_{LCO} is earlier than satellite-derived D_{LCO}; R = Pearson's correlation coefficient; RMSE = root mean square error.

TABLE 1 Proportions of years with possible cold events before D_{LCO} (for satellite and *in situ* observations) and before D_{PDO} (for FLUXNET2015)

Metrics	Satellite D_{LCO} (2000–2016)	*In situ* D_{LCO} China	FLUXNET2015 D_{PDO}
Proportion (%) of years with possible cold events (0°C)	1.6	1.7	.6
Proportion (%) of years with possible cold events (2°C)	2.1	3.5	1.0

Note: Possible cold events were determined mainly by using a threshold-based method with a daily minimum temperature of 0 or 2°C (for identification of possible cold events, see Section 2.4.5).

Abbreviations: D_{LCO}, timing of onset of leaf coloration in autumn; D_{PDO}, timing of onset of the decrease in maximum canopy photosynthetic capacity in autumn.

13% of the area, mainly in the temperate grassland of North America and in the middle latitudes of Eurasia, sub-arctic grassland, and alpine steppe of the Tibetan Plateau (Supporting Information Figure S9). Therefore, neither pre-D_{LCO} T_{min} nor precipitation was a useful predictor of D_{LCO} in most areas. We obtained similar results when using the month preceding D_{LCO} (Supporting Information Figure S10) or 15 days preceding D_{LCO} (Supporting Information Figure S11) as the pre-D_{LCO} period, with only 6 and 5%, respectively, of the area showing a significant positive correlation between D_{LCO} and pre-D_{LCO} T_{min}. We also investigated the relationship between D_{LCO} and the lowest daily minimum temperature during the 15 days before the multiyear mean D_{LCO}, and only 3% of the area showed a significant positive correlation (Supporting Information Figure S12). Moreover, including the date of onset of green-up as an extra control variable in the partial correlation analyses did not affect the results (Supporting Information Figure S13). The *in situ* phenological records in China indicated that ground-observed D_{LCO} was positively correlated with pre-D_{LCO} T_{min} for 13% of the time series and was not correlated with pre-D_{LCO} T_{min} for 82% of the time series (Table 2). Excluding D_{LCO} possibly caused by cold events produced similar results (Supporting Information Figure S14; Table S6). Overall, these results suggest that an increase in pre-D_{LCO} T_{min} is not likely to delay D_{LCO} in most areas in the middle and high northern latitudes.

3.5 | Impacts of temperature on the progress of leaf coloration

We first examined whether the timings of earlier stages of leaf coloration are less closely related to temperature than later stages. The fact that the earlier stages of leaf coloration had fewer areas with a significantly delayed trend (Supporting Information Figure S8) is in agreement with the finding that the significantly positive correlations between the timings of earlier stages of leaf coloration and T_{min} were observed in fewer areas (Figure 4c). The timings of leaf coloration stage corresponding to NDVI decreases by 40, 30, 20 and

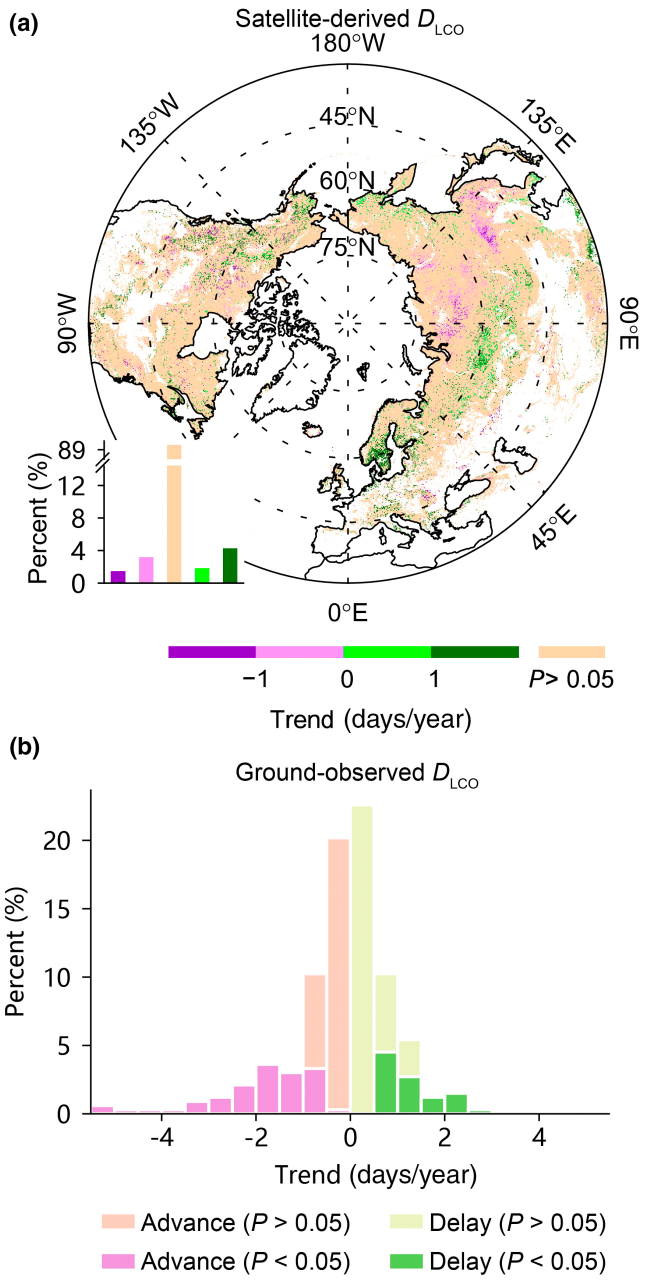

FIGURE 3 Temporal trends in the timing of the onset of leaf coloration (D_{LCO}), as retrieved from satellite and *in situ* observations. (a) Satellite-derived D_{LCO} trends over 2000–2018. The bar chart in the bottom-left corner shows the percentage of area within each interval of the significant temporal trends and the percentage of area with non-significant trends, indicated by the colour scale at the bottom. Positive and negative trend values refer to significantly delayed and advanced D_{LCO}, respectively. D_{LCO} corresponds to a 10% decrease in normalized difference vegetation index. (b) Ground-observed D_{LCO} trends derived over 1971–1997 from observations of *in situ* leaf coloration in China. Significant temporal trends were determined using *t* tests at $p < .05$ and ordinary least squares regression.

10% (i.e., D_{LCO}) exhibited a significant positive correlation with T_{min} in 30, 25, 17 and 9% of the area, respectively (Figure 4a,c; Supporting Information Figure S15). In particular, D_{LCE} exhibited a significant

positive correlation with pre-D_{LCE} T_{min} in 34% of the area (Figure 4b), substantially more than that for the D_{LCO}–T_{min} correlations (9%; Figure 4a). The proportion increased to 38 and 41% for the timings of leaf coloration stage corresponding to a 60 and 90% decrease in NDVI, respectively (Supporting Information Figure S16).

These results show decreasing correlations with temperature of earlier stages of leaf senescence. To verify this, we examined the correlation between D_{PDO}, an indicator of leaf senescence earlier than D_{LCO}, and pre-D_{PDO} T_{min}. D_{PDO} and pre-D_{PDO} T_{min} exhibited a less positive correlation than NDVI-derived D_{LCO} and pre-D_{LCO} T_{min} at the same sites during the same periods (3 and 6% of the sites for D_{PDO} and D_{LCO}, respectively; Supporting Information Table S7). Among all the eddy-covariance towers, D_{LCO} exhibited a significant positive correlation with pre-D_{LCO} T_{min} in 3% of the 36 and was not correlated with pre-D_{PDO} T_{min} in 89% of the eddy-covariance records (Table 2). Moreover, excluding D_{PDO} possibly caused by cold events produced similar results (Supporting Information Table S6).

We then examined whether D_{LCO} is less sensitive to temperature than D_{LCE}. In most regions (66%) of the middle and high northern latitudes, the temperature sensitivity of D_{LCO} was less than that of D_{LCE} (Figure 4d). The temperature sensitivity of D_{LCO} was less than D_{LCE} by ≥4 days/°C in 39% of the study area, mainly in northern Europe, the eastern USA, eastern Canada and western Russia. In 14% of the area, the temperature sensitivity of D_{LCO} was >4 days/°C greater than D_{LCE}, mainly distributed in the Tibetan Plateau, western North America, areas in Europe near 60° N, northern Kazakhstan, and between 45 and 65° N in Russia.

As can be expected from the lower temperature sensitivity of D_{LCO} relative to that of D_{LCE}, warming could extend the duration of leaf coloration in 71% of the area (Figure 4e). In 42% of the area, the temperature sensitivity of the duration of leaf coloration was >3 days/°C, mainly in Russia, eastern North America and northern Europe. The area with a temperature sensitivity <−3 days/°C accounted for 11% of the study area, scattered in the Tibetan Plateau, central USA, western North America, between 45 and 60° N in Europe, northern Kazakhstan and south-eastern Russia.

Moreover, warming could slow the progress of leaf coloration. In 69% of the area, the speed of leaf coloration could be reduced by higher temperature (Figure 4f), particularly in the region north of 60° N. The temperature sensitivity of the speed of leaf coloration was <−1‰/day/°C in 34% of the study area (negative values of temperature sensitivity indicate that warming reduces the speed of leaf coloration), mainly in eastern and northern Canada, northern Europe and northern Russia. Only 13% of the area showed a large increase in the speed of leaf coloration under increasing temperature (>1‰/day/°C), scattered in Mongolia, the Tibetan Plateau, western Canada, central and western USA, and central and south-eastern Russia.

When considering early summer NDVI decline, we also found that more advanced stages of leaf coloration were more responsive to temperature (Supporting Information Figures S17c,d and S18c,d), and that warming could slow the progress of coloration (Supporting Information Figures S17f and S18f) and extend the duration of leaf coloration (Supporting Information Figures S17e and S18e).

3.6 | Dependence of D_{LCO} on daylength

We attempted to explore the dependence of D_{LCO} on daylength by examining the variabilities in the correlation between D_{LCO} and T_{min} and in temporal changes in D_{LCO} against the spatial gradient of daylength. In the areas with longer daylengths at multiyear mean D_{LCO}, there were proportionally fewer significant D_{LCO} delays during 2000–2018 (Figure 5a; Supporting Information Figure S19a), and the positive relationship between D_{LCO} and pre-D_{LCO} T_{min} was slightly weaker, as indicated by the lower partial correlation coefficient between them (Figure 5d). Such patterns were more prominent for woody vegetation than for herbaceous vegetation (Figure 5b,c,e,f; Supporting Information Figure S19b,c). For vegetation with a daylength at D_{LCO} of >13.5 h, D_{LCO} was more positively correlated with pre-D_{LCO} T_{min} in colder areas at a given daylength (Figure 5d–f). The dependences of D_{LCO} trends on daylength and of the correlation between D_{LCO} and pre-D_{LCO} T_{min} on daylength were also found when years with possible cold events before D_{LCO} were excluded (Supporting Information Figure S20) and when we considered summer decline in NDVI (Supporting Information Figures S21 and S22). The correlation between D_{LCO} and pre-D_{LCO} total precipitation was independent of daylength and was slightly stronger for the areas with a higher temperature before D_{LCO}, mostly because of the

FIGURE 4 Impacts of temperature on the timing of different stages of leaf coloration and on the progress of leaf coloration over the period 2000–2018. (a) Spatial pattern of the partial correlation coefficient (R_{TN}) between the onset of leaf coloration [D_{LCO}, 10% decrease in normalized difference vegetation index (NDVI)] and pre-D_{LCO} mean daily minimum temperature (T_{min}). (b) Spatial pattern of R_{TN} between timing of the end of leaf coloration (D_{LCE}, 50% decrease in NDVI) and pre-D_{LCE} T_{min}. The bar charts inset in (a) and (b) show the percentage of area for each interval of the partial correlation coefficient ($p < .05$), with the coefficient indicated by the colour scale on the right. Non-significant correlations ($p > .05$) are in grey. (c) Percentage of area for which R_{TN} between the timing of a given stage of leaf coloration and preceding T_{min} is higher than a given threshold indicated by the horizontal axis. For example, R_{TN} for the onset of leaf coloration is >.2 in *c*. 40% of the area. (d) Difference in temperature sensitivity between D_{LCE} and D_{LCO}. Positive values indicate that D_{LCE} is more sensitive to temperature than D_{LCO}, whereas negative values indicate that D_{LCO} is more sensitive to temperature than D_{LCE}. (e) Temperature sensitivity of the duration of leaf coloration. Positive values indicate that warming extends the duration of leaf coloration, whereas negative values indicate that warming shortens the leaf coloration duration. (f) Temperature sensitivity of the speed of leaf coloration. Positive values indicate that warming increases the speed of leaf coloration, whereas negative values indicate that warming reduces the speed of leaf coloration. The bar charts inset in (d–f) show the percentage of area for each interval of the temperature sensitivity indicated by the colour scale on the right.

Global Ecology and Biogeography A Journal of Macroecology

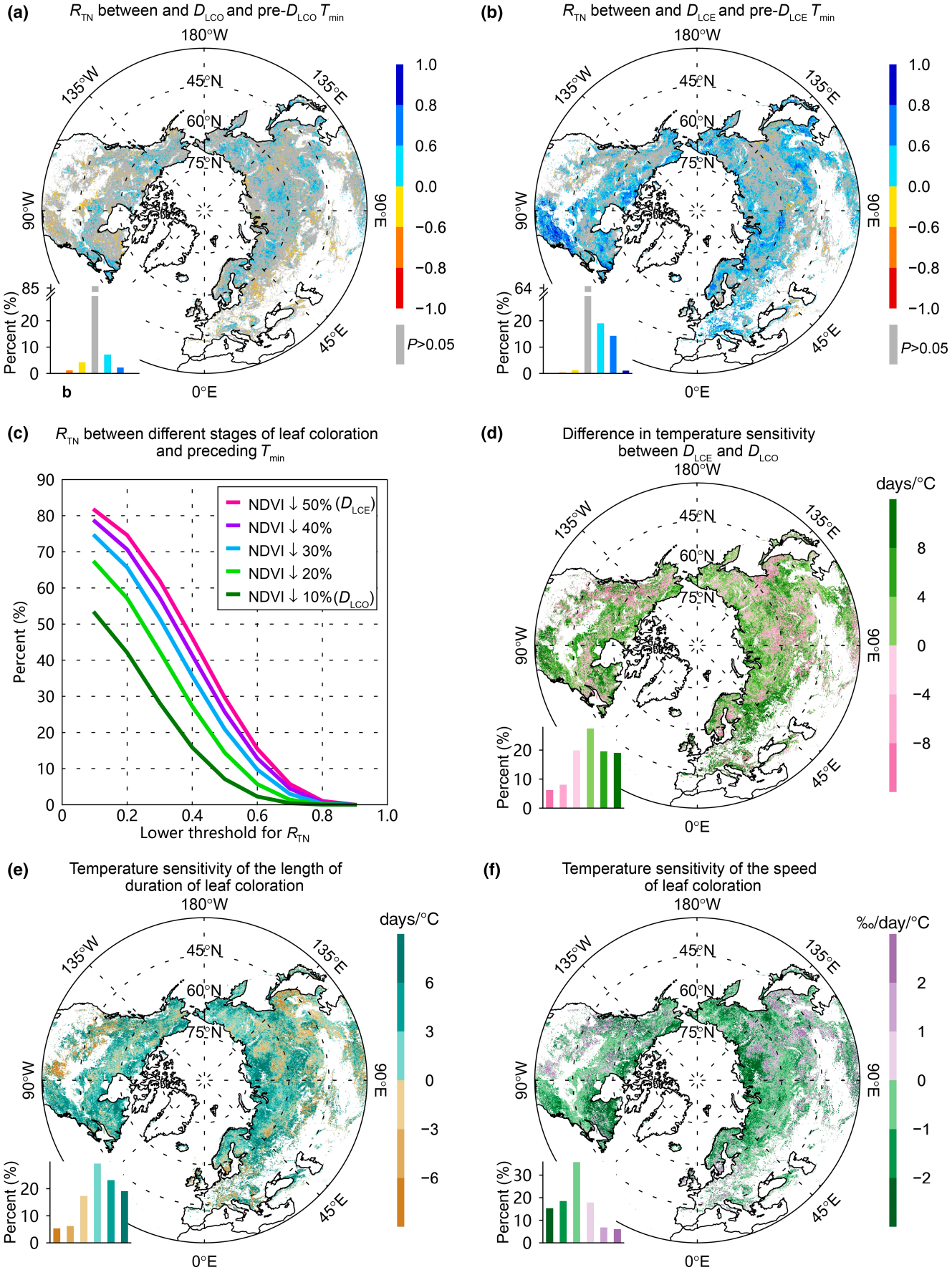

TABLE 2 Percentage of correlations between D_{LCO} or D_{PDO} and each climate factor for each interval of the partial correlation coefficient

Metric	Number of time series	Climate factor	Interval of the partial correlation coefficient ($p < .05$)						
			(−1.0, −.8)	(−.8, −.6)	(−.6, 0)	(0, .6)	(.6, .8)	(.8, 1.0)	$p > .05$
In situ D_{LCO} China	332	Temperature	0	2	3	4	8	1	82
		Precipitation	0	3	3	4	5	0	85
FLUXNET2015 D_{PDO}	36	Temperature	0	5	3	0	3	0	89
		Precipitation	0	6	0	8	3	5	78

Note: The data in the rightmost column indicate the percentages of area or time series with non-significant correlations.

Abbreviations: D_{LCO}, timing of the onset of leaf coloration in autumn; D_{PDO}, timing of the onset of the decrease in maximum canopy photosynthetic capacity in autumn.

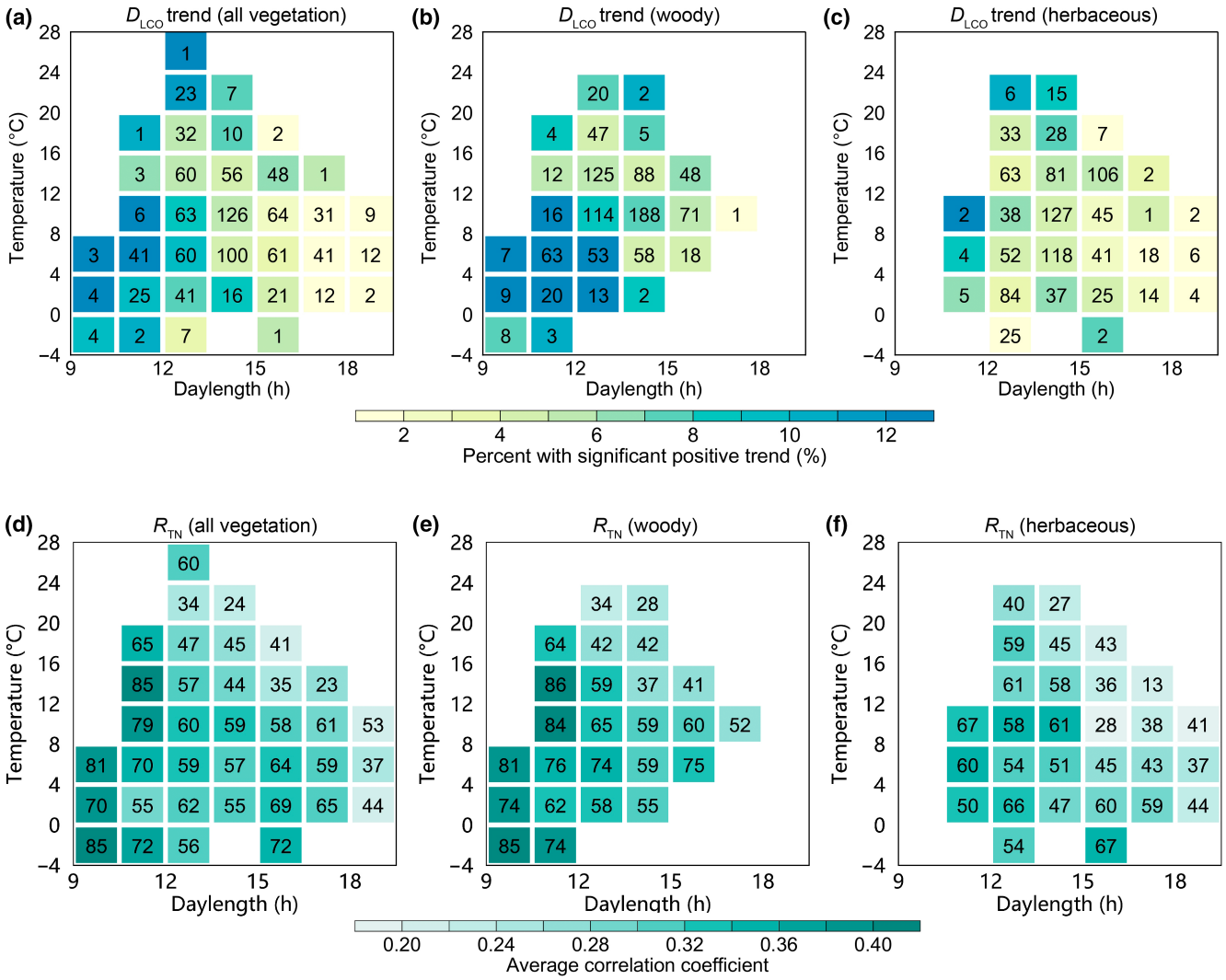

FIGURE 5 Dependence of temporal trends in the timing of the onset of leaf coloration [D_{LCO}, 10% decrease in normalized difference vegetation index (NDVI); a–c] and of the partial correlation coefficient (R_{TN}; d–f) between D_{LCO} and pre-D_{LCO} mean daily minimum temperature (T_{min}) on daylength and temperature over the period 2000–2018. (a) All vegetation. Colour indicates the percentage of area with significant ($p < .05$) D_{LCO} delays in each cell (i.e., a specific temperature × daylength combination), as indicated in the scale at the bottom. The number in each cell indicates the ratio (unit: ‰) of the area in each cell to the total area with D_{LCO} retrieval. The temporal trends and their significances were determined with ordinary least squares regression and *t* tests. (b,c) The same as (a), but for woody and herbaceous vegetation, respectively. (d) All vegetation. Colour indicates the average of the positive R_{TN}, as indicated in the scale at the bottom. The number in each cell indicates the percentage of area with a positive correlation in each cell. (e,f) The same as (d), but for woody and herbaceous vegetation, respectively. Only cells where the ratio of the area of the cell to the total area is >1‰ are represented.

stronger effect of precipitation in delaying D_{LCO} in herbaceous vegetation (Supporting Information Figures S9 and S23).

4 | DISCUSSION

In previous analyses of *in situ* and satellite observations (Garonna et al., 2014; Gill et al., 2015; Liu et al., 2016), the advanced stage of autumnal leaf senescence, indicated by D_{LCE}, was significantly delayed in a larger proportion of areas, or time series, than was D_{LCO} in our study. In the present study, D_{LCE} was also significantly delayed in more areas than D_{LCO} (Supporting Information Figure S8), probably because the timings of the earlier stages of leaf coloration determined from satellite data were less affected by T_{min} than the later stages (Figure 4a–c; Supporting Information Figure S15). Evidence for photoperiodic control of the start of leaf senescence (Fracheboud et al., 2009; Keskitalo et al., 2005) suggests that the early phases of leaf senescence are insensitive to warming, in contrast to the later phases. Given that the degradation of chlorophyll starts earlier than leaf coloration (Lim et al., 2007; Tang et al., 2016), the timing of autumnal phenological metrics that closely follow chlorophyll degradation before D_{LCO} should be less delayed by temperature increase than D_{LCO} if chlorophyll degradation is triggered by the photoperiod. In our analysis, we verified that D_{PDO} was less positively correlated with temperature than D_{LCO} (Supporting Information Table S7), probably because the start of autumnal chlorophyll degradation was controlled by photoperiod and was not delayed by higher temperature (Bauerle et al., 2012; Fracheboud et al., 2009; Keskitalo et al., 2005).

Overall, our results suggest that temperature does not initiate senescence in autumn in most areas; instead, it influences the speed of change in coloration after it starts (Figure 4f) (Fracheboud et al., 2009). The lack of a positive correlation between D_{LCO} (or D_{PDO}) and pre-D_{LCO} (or pre-D_{PDO}) temperature suggests an overriding photoperiodic control that makes the timing of the onset of leaf senescence stable. In the areas with longer daylengths (calculated for each pixel/location at multiyear mean D_{LCO} over 2000–2018), there were proportionally fewer significant D_{LCO} delays during 2000–2018 (Figure 5a; Supporting Information Figure S19a), and the positive relationship between D_{LCO} and pre-D_{LCO} T_{min} was slightly weaker, as indicated by the smaller partial correlation coefficient between them (Figure 5d). Such dependences on daylength were more prominent for woody vegetation than for herbaceous vegetation (Figure 5b,c,e,f; Supporting Information Figure S19b,c), in agreement with experimental findings suggesting that the initiation of leaf senescence in woody plants is likely to be controlled by photoperiod (Fracheboud et al., 2009; Keskitalo et al., 2005). These findings indicate stronger photoperiodic control in areas where daylength at D_{LCO} is longer (i.e., shorter nights), possibly because plants respond to the duration of uninterrupted darkness rather than daylength (Borthwick & Hendricks, 1960; Hamner, 1940; Howe et al., 1995; Paus et al., 1986). Interestingly, for vegetation with a daylength at D_{LCO} of >13.5 h, D_{LCO} was more positively correlated with pre-D_{LCO} T_{min} in colder areas (Figure 5d–f), indicating a stronger effect of temperature in areas with harsh temperature conditions, consistent with experimental studies (Ford et al., 2017; Zohner et al., 2016). Therefore, although for these types of vegetation the correlation between D_{LCO} and temperature is weak, probably because of stronger photoperiodic control, there is still a signal of temperature influence on D_{LCO}, reflecting a stronger selection pressure in harsher temperature environments.

Although observational evidence is limited, experimental results have been reported for the photoperiodic induction of leaf senescence in several, mostly woody, species (Supporting Information Table S1). However, in those manipulative experiments, daylength was altered by several hours (>4 h; Supporting Information Table S1), which is more extreme than the natural conditions plants are likely to experience. Daylength depends only on the day of year and location. Owing to the interannual limited variations in the timings of leaf coloration or senescence onset, the fluctuation in daylength in natural conditions is far less than that in manipulative experiments. Therefore, the role of photoperiod in leaf senescence identified in such experimental conditions does not necessarily apply to plants in natural conditions. The results in the present study support experimental findings in wild plants at the biome and continental scales and show that photoperiod influences the onset of leaf coloration, which closely follows the initiation of leaf senescence.

Autumnal leaf senescence in preparation for overwintering is an evolutionary trade-off between the re-allocation of leaf nutrients before leaf shed to reduce the risk of frost damage and the assimilation of carbon (Estiarte & Peñuelas, 2015). The response of leaf senescence to an increase in temperature in autumn influences this trade-off. The absence of delays over time in the onset of leaf coloration and in the onset of decrease in maximum canopy photosynthetic capacity in response to climate warming, as observed in our study, might limit the detrimental effects of frost in autumn (Liu et al., 2018) and might also have limited impacts on the start of the remobilization and resorption of nutrients (Estiarte & Peñuelas, 2015). The slower rate of progress of leaf senescence (Figure 4f) and extended duration of leaf coloration (Figure 4e) under warming might increase the efficiency of nitrogen resorption (Rennenberg et al., 2010) and increase the vegetation greenness in this period, which will modify the surface energy balance through biophysical processes (Shen et al., 2015). The extended period of leaf coloration might also prolong the plant transpiration time and increase soil water consumption. The impact of autumn warming on net ecosystem productivity is dual, increasing both respiratory flux to the atmosphere (Piao et al., 2008) and forest gross primary photosynthesis (Keenan et al., 2014). The relatively static onset date of leaf coloration and its weak response to temperature would preclude the vegetation from fully using the potential increase in CO_2 assimilation in early autumn induced by warming (Stinziano & Way, 2017). Combined with a delay in the end of the season and an increase in respiration attributable to warming, this suggests that additional warming will probably not result in a continuous increase in autumn CO_2 assimilation.

In summary, satellite NDVI time series and ground-based phenological observations indicated no significant delay in the start of

autumnal leaf coloration for most areas covered by natural vegetation over middle and high northern latitudes. Neither pre-D_{LCO} temperature nor pre-D_{LCO} precipitation significantly affected the interannual variations of the start of leaf coloration in most areas, indicating that the start of leaf senescence is triggered by photoperiod. Interestingly, there was a weaker positive correlation between the start of autumnal leaf coloration and pre-D_{LCO} T_{min} for vegetation in regions with longer daylength, indicating strong photoperiodic control of the start of leaf senescence. For vegetation with a given daylength at D_{LCO} >13.5 h, the positive correlation between D_{LCO} and pre-D_{LCO} T_{min} was slightly stronger in colder areas, suggesting that there is strong selection pressure in harsher temperature environments on the timing of leaf coloration onset, and that autumn warming could have a stronger delaying effect on leaf coloration onset in colder areas than in warmer areas. This study suggests that autumnal warming will not change the start date of leaf senescence, but it might slow the rate of senescence. A slower senescence speed might extend the period of senescence and provide more time to re-allocate nutrients and prepare for overwintering. Such changes could substantially affect carbon and nutrient cycles. Our study provides a foundation for understanding the complex relationships among nutrient cycling, vegetation growth, energy exchange and climate change in autumn in temperate and boreal regions dominated by winter deciduous vegetation.

AUTHOR CONTRIBUTIONS

M.S. designed the research and conceived the study; N.J. and M.S. performed the research; N.J. analysed the data; and all the authors interpreted the results and wrote the paper.

ACKNOWLEDGMENTS

This work was funded by the Second Scientific Expedition to the Qinghai-Tibet Plateau (no. 2019QZKK0307) and the Fundamental Research Funds for the Central Universities. M.C. wishes to acknowledge the ERC Starting Grant LEAF-FALL (714916). J.P. acknowledges financial support from the European Research Council Synergy (grant no. ERC-SyG-2013-610028 IMBALANCE-P). L.Š. was supported by the Ministry of Education, Youth and Sports of the Czech Republic within the CzeCOS programme (grant no. LM2015061) and by SustES—Adaptation Strategies for Sustainable Ecosystem Services and Food Security Under Adverse Environmental Conditions (project no. CZ.02.1.01/0.0/0.0/16_019/0000797).

DATA AVAILABILITY STATEMENT

All data used for this study are publicly available online. The satellite reflectance products at .05° resolution (MOD09CMG) used to estimate phenological metrics and the global land cover map (MCD12C1–2009) used to identify natural vegetation are freely available online at: https://ladsweb.modaps.eosdis.nasa.gov. The PhenoCam data (PhenoCam Dataset v.2.0) used to evaluate the satellite-derived phenological metrics are available at: https://doi.org/10.3334/ORNLDAAC/1674; and the subsets of satellite reflectance products at 500-m resolution (MOD09A1) at PhenoCam sites are downloaded from: https://modis.ornl.gov/globalsubset/. The climatic data for the region are publicly available: CRU TS 4.03 monthly climatic data are available via http://data.ceda.ac.uk; and CRU-NCEP v.7.2 6-hourly climatic data are available via https://vesg.ipsl.upmc.fr. *In situ* phenological observations in China are available from the National Earth System Science Data Sharing Infrastructure, National Science and Technology Infrastructure of China (http://www.geodata.cn). The climatic data of *in situ* observations in China are available from National Meteorological Information Center (http://data.tpdc.ac.cn). The site-based gross primary productivity products used to estimate phenological metrics and the corresponding half-hourly climatic data are extracted from the FLUXNET2015 Dataset (http://fluxnet.fluxdata.org/data/fluxnet2015-dataset/). The source code of the spatial–temporal Savitzky–Golay filter is available at: https://github.com/cao-sre/STSG_IDL_program. The codes for analyses are available from figshare (https://figshare.com/s/be760555bb74ef0e6bf2).

ORCID

Nan Jiang https://orcid.org/0000-0001-5151-5715
Miaogen Shen https://orcid.org/0000-0001-5742-8807
Shilong Piao https://orcid.org/0000-0001-8057-2292
Eryuan Liang https://orcid.org/0000-0002-8003-4264

REFERENCES

Bauerle, W. L., Oren, R., Way, D. A., Qian, S. S., Stoy, P. C., Thornton, P. E., Bowden, J. D., Hoffman, F. M., & Reynolds, R. F. (2012). Photoperiodic regulation of the seasonal pattern of photosynthetic capacity and the implications for carbon cycling. *Proceedings of the National Academy of Sciences of the United States of America*, *109*(22), 8612–8617. https://doi.org/10.1073/pnas.1119131109

Beck, P. S. A., Atzberger, C., Høgda, K. A., Johansen, B., & Skidmore, A. K. (2006). Improved monitoring of vegetation dynamics at very high latitudes: A new method using MODIS NDVI. *Remote Sensing of Environment*, *100*(3), 321–334. https://doi.org/10.1016/j.rse.2005.10.021

Berman, E. E., Graves, T. A., Mikle, N. L., Merkle, J. A., Johnston, A. N., & Chong, G. W. (2020). Comparative quality and trend of remotely sensed phenology and productivity metrics across the western United States. *Remote Sensing*, *12*(16), 2538. https://doi.org/10.3390/rs12162538

Borthwick, H. A., & Hendricks, S. B. (1960). Photoperiodism in plants. *Science*, *132*(3435), 1223–1228. https://doi.org/10.1126/science.132.3435.1223

Buitenwerf, R., Rose, L., & Higgins, S. I. (2015). Three decades of multi-dimensional change in global leaf phenology. *Nature Climate Change*, *5*(4), 364–368. https://doi.org/10.1038/nclimate2533

Cao, R., Chen, Y., Shen, M., Chen, J., Zhou, J., Wang, C., & Yang, W. (2018). A simple method to improve the quality of NDVI time-series data by integrating spatiotemporal information with the Savitzky-Golay filter. *Remote Sensing of Environment*, *217*, 244–257. https://doi.org/10.1016/j.rse.2018.08.022

Chen, J., Rao, Y., Shen, M., Wang, C., Zhou, Y., Ma, L., Tang, Y., & Yang, X. (2016). A simple method for detecting phenological change from time series of vegetation index. *IEEE Transactions on Geoscience and Remote Sensing*, *54*(6), 3436–3449. https://doi.org/10.1109/TGRS.2016.2518167

China Meteorological Administration. (1993). *Observation criterion of agricultural meteorology*. China Meteorological Press (in Chinese).

Cong, N., Shen, M., & Piao, S. (2017). Spatial variations in responses of vegetation autumn phenology to climate change on the

Tibetan Plateau. *Journal of Plant Ecology*, *10*, 744–752. https://doi.org/10.1093/jpe/rtw084

Delpierre, N., Dufrêne, E., Soudani, K., Ulrich, E., Cecchini, S., Boé, J., & François, C. (2009). Modelling interannual and spatial variability of leaf senescence for three deciduous tree species in France. *Agricultural and Forest Meteorology*, *149*(6), 938–948. https://doi.org/10.1016/j.agrformet.2008.11.014

Elmore, A. J., Guinn, S. M., Minsley, B. J., & Richardson, A. D. (2012). Landscape controls on the timing of spring, autumn, and growing season length in mid-Atlantic forests. *Global Change Biology*, *18*(2), 656–674. https://doi.org/10.1111/j.1365-2486.2011.02521.x

Estiarte, M., & Peñuelas, J. (2015). Alteration of the phenology of leaf senescence and fall in winter deciduous species by climate change: Effects on nutrient proficiency. *Global Change Biology*, *21*(3), 1005–1017. https://doi.org/10.1111/gcb.12804

Estrella, N., & Menzel, A. (2006). Responses of leaf colouring in four deciduous tree species to climate and weather in Germany. *Climate Research*, *32*(3), 253–267.

Ford, K. R., Harrington, C. A., & Clair, J. B. S. (2017). Photoperiod cues and patterns of genetic variation limit phenological responses to climate change in warm parts of species' range: Modeling diameter-growth cessation in coast Douglas-fir. *Global Change Biology*, *23*(8), 3348–3362. https://doi.org/10.1111/gcb.13690

Fracheboud, Y., Luquez, V., Björkén, L., Sjödin, A., Tuominen, H., & Jansson, S. (2009). The control of autumn senescence in European aspen. *Plant Physiology*, *149*(4), 1982–1991. https://doi.org/10.1104/pp.108.133249

Friedl, M., & Sulla-Menashe, D. (2015). *MCD12C1 MODIS/Terra+Aqua Land Cover Type Yearly L3 Global 0.05Deg CMG V006 [Data set]. NASA EOSDIS Land Processes DAAC*. https://doi.org/10.5067/MODIS/MCD12C1.006

Fu, Y. H., Zhang, X., Piao, S., Hao, F., Geng, X., Vitasse, Y., Zohner, C., Peñuelas, J., & Janssens, I. A. (2019). Daylength helps temperate deciduous trees to leaf-out at the optimal time. *Global Change Biology*, *25*(7), 2410–2418. https://doi.org/10.1111/gcb.14633

Fu, Y. H., Zhao, H., Piao, S., Peaucelle, M., Peng, S., Zhou, G., Ciais, P., Huang, M., Menzel, A., Peñuelas, J., Song, Y., Vitasse, Y., Zeng, Z., & Janssens, I. A. (2015). Declining global warming effects on the phenology of spring leaf unfolding. *Nature*, *526*(7571), 104–107. https://doi.org/10.1038/nature15402

Fu, Y. S. H., Campioli, M., Vitasse, Y., De Boeck, H. J., Van den Berge, J., AbdElgawad, H., Asard, H., Piao, S., Deckmyn, G., & Janssens, I. A. (2014). Variation in leaf flushing date influences autumnal senescence and next year's flushing date in two temperate tree species. *Proceedings of the National Academy of Sciences of the United States of America*, *111*(20), 7355–7360. https://doi.org/10.1073/pnas.1321727111

Gan, S. S., & Amasino, R. M. (1997). Making sense of senescence - Molecular genetic regulation and manipulation of leaf senescence. *Plant Physiology*, *113*(2), 313–319. https://doi.org/10.1104/pp.113.2.313

Ganguly, S., Friedl, M. A., Tan, B., Zhang, X., & Verma, M. (2010). Land surface phenology from MODIS: Characterization of the collection 5 global land cover dynamics product. *Remote Sensing of Environment*, *114*(8), 1805–1816. https://doi.org/10.1016/j.rse.2010.04.005

Gao, M., Piao, S., Chen, A., Yang, H., Liu, Q., Fu, Y. H., & Janssens, I. A. (2019). Divergent changes in the elevational gradient of vegetation activities over the last 30 years. *Nature Communications*, *10*(1), 2970. https://doi.org/10.1038/s41467-019-11035-w

Garonna, I., De Jong, R., De Wit, A. J. W., Mücher, C. A., Schmid, B., & Schaepman, M. E. (2014). Strong contribution of autumn phenology to changes in satellite-derived growing season length estimates across Europe (1982–2011). *Global Change Biology*, *20*(11), 3457–3470.

Ge, Q. S., Wang, H. J., Rutishauser, T., & Dai, J. H. (2015). Phenological response to climate change in China: A meta-analysis. *Global Change Biology*, *21*(1), 265–274.

Gill, A. L., Gallinat, A. S., Sanders-DeMott, R., Rigden, A. J., Short Gianotti, D. J., Mantooth, J. A., & Templer, P. H. (2015). Changes in autumn senescence in northern hemisphere deciduous trees: A meta-analysis of autumn phenology studies. *Annals of Botany*, *116*(6), 875–888. https://doi.org/10.1093/aob/mcv055

Gu, L., Post, W. M., Baldocchi, D. D., Black, T. A., Suyker, A. E., Verma, S. B., Vesala, T., & Wofsy, S. C. (2009). Characterizing the seasonal dynamics of plant community photosynthesis across a range of vegetation types. In A. Noormets (Ed.), *Phenology of ecosystem processes* (pp. 35–58). Springer.

Hamner, K. C. (1940). Interrelation of light and darkness in photoperiod. *Botanical Gazette*, *101*(3), 658–687.

Harris, I., Jones, P. D., Osborn, T. J., & Lister, D. H. (2014). Updated high-resolution grids of monthly climatic observations – the CRU TS3.10 Dataset. *International Journal of Climatology*, *34*(3), 623–642. https://doi.org/10.1002/joc.3711

Howe, G. T., Hackett, W. P., Furnier, G. R., & Klevorn, R. E. (1995). Photoperiodic responses of a northern and southern ecotype of black cottonwood. *Physiologia Plantarum*, *93*(4), 695–708.

Jeganathan, C., Dash, J., & Atkinson, P. M. (2014). Remotely sensed trends in the phenology of northern high latitude terrestrial vegetation, controlling for land cover change and vegetation type. *Remote Sensing of Environment*, *143*, 154–170. https://doi.org/10.1016/j.rse.2013.11.020

Jeong, S. J., Ho, C. H., Gim, H. J., & Brown, M. E. (2011). Phenology shifts at start vs. end of growing season in temperate vegetation over the Northern Hemisphere for the period 1982–2008. *Global Change Biology*, *17*(7), 2385–2399.

Keenan, T. F., Gray, J., Friedl, M. A., Toomey, M., Bohrer, G., Hollinger, D. Y., Munger, J. W., O'Keefe, J., Schmid, H. P., Wing, I. S., Yang, B., & Richardson, A. D. (2014). Net carbon uptake has increased through warming-induced changes in temperate forest phenology. *Nature Climate Change*, *4*(7), 598–604. https://doi.org/10.1038/nclimate2253

Keenan, T. F., & Richardson, A. D. (2015). The timing of autumn senescence is affected by the timing of spring phenology: Implications for predictive models. *Global Change Biology*, *21*(7), 2634–2641. https://doi.org/10.1111/gcb.12890

Keskitalo, J., Bergquist, G., Gardeström, P., & Jansson, S. (2005). A cellular timetable of autumn senescence. *Plant Physiology*, *139*(4), 1635–1648. https://doi.org/10.1104/pp.105.066845

Klosterman, S., & Richardson, A. D. (2017). Observing spring and fall phenology in a deciduous forest with aerial drone imagery. *Sensors (Basel)*, *17*(12), 2852. https://doi.org/10.3390/s17122852

Klosterman, S. T., Hufkens, K., Gray, J. M., Melaas, E., Sonnentag, O., Lavine, I., Mitchell, L., Norman, R., Friedl, M. A., & Richardson, A. D. (2014). Evaluating remote sensing of deciduous forest phenology at multiple spatial scales using PhenoCam imagery. *Biogeosciences*, *11*(16), 4305–4320. https://doi.org/10.5194/bg-11-4305-2014

Körner, C. (2007). Significance of temperature in plant life. In J. I. L. Morison & M. D. Morecroft (Eds.), *Plant growth and climate change* (pp. 48–69). Blackwell Publishing Ltd.

Körner, C. (2021). *Alpine plant life: Functional plant ecology of high mountain ecosystems*. Springer International Publishing.

Körner, C., & Basler, D. (2010). Response-warming, photoperiods, and tree phenology. *Science*, *329*(5989), 278. https://doi.org/10.1126/science.329.5989.278

Körner, C., & Hiltbrunner, E. (2018). The 90 ways to describe plant temperature. *Perspectives in Plant Ecology, Evolution and Systematics*, *30*, 16–21. https://doi.org/10.1016/j.ppees.2017.04.004

Leblans, N. I. W., Sigurdsson, B. D., Vicca, S., Fu, Y. S., Penuelas, J., & Janssens, I. A. (2017). Phenological responses of Icelandic subarctic grasslands to short-term and long-term natural soil warming. *Global Change Biology*, *23*(11), 4932–4945.

Lenz, A., Hoch, G., Vitasse, Y., & Körner, C. (2013). European deciduous trees exhibit similar safety margins against damage by spring freeze events along elevational gradients. *New Phytologist*, *200*(4), 1166–1175. https://doi.org/10.1111/nph.12452

Lim, P. O., Kim, H. J., & Nam, H. G. (2007). Leaf senescence. *Annual Review of Plant Biology*, *58*, 115–136 1543-5008/07/0602-0115$20.00.

Liu, Q., Fu, Y. H., Zhu, Z., Liu, Y., Liu, Z., Huang, M., Janssens, I. A., & Piao, S. (2016). Delayed autumn phenology in the Northern Hemisphere is related to change in both climate and spring phenology. *Global Change Biology*, *22*(11), 3702–3711.

Liu, Q., Piao, S., Janssens, I. A., Fu, Y., Peng, S., Lian, X., Ciais, P., Myneni, R. B., Peñuelas, J., & Wang, T. (2018). Extension of the growing season increases vegetation exposure to frost. *Nature Communications*, *9*(1), 426. https://doi.org/10.1038/s41467-017-02690-y

Lukasová, V., Bucha, T., Škvareninová, J., & Škvarenina, J. (2019). Validation and application of European beech phenological metrics derived from MODIS data along an altitudinal gradient. *Forests*, *10*(1), 60.

Mariën, B., Balzarolo, M., Dox, I., Leys, S., Lorène, M. J., Geron, C., Portillo-Estrada, M., AbdElgawad, H., Asard, H., & Campioli, M. (2019). Detecting the onset of autumn leaf senescence in deciduous forest trees of the temperate zone. *New Phytologist*, *224*(1), 166–176.

Matsumoto, K., Ohta, T., Irasawa, M., & Nakamura, T. (2003). Climate change and extension of the *Ginkgo biloba* L. growing season in Japan. *Global Change Biology*, *9*(11), 1634–1642. https://doi.org/10.1046/j.1365-2486.2003.00688.x

Melaas, E. K., Friedl, M. A., & Zhu, Z. (2013). Detecting interannual variation in deciduous broadleaf forest phenology using Landsat TM/ETM+data. *Remote Sensing of Environment*, *132*, 176–185. https://doi.org/10.1016/j.rse.2013.01.011

Menzel, A., Yuan, Y., Matiu, M., Sparks, T., Scheifinger, H., Gehrig, R., & Estrella, N. (2020). Climate change fingerprints in recent European plant phenology. *Global Change Biology*, *26*(4), 2599–2612. https://doi.org/10.1111/gcb.15000

Morisette, J. T., Richardson, A. D., Knapp, A. K., Fisher, J. I., Graham, E. A., Abatzoglou, J., Wilson, B. E., Breshears, D. D., Henebry, G. M., Hanes, J. M., & Liang, L. (2009). Tracking the rhythm of the seasons in the face of global change: Phenological research in the 21st century. *Frontiers in Ecology and the Environment*, *7*(5), 253–260. https://doi.org/10.1890/070217

Myneni, R. B., Keeling, C. D., Tucker, C. J., Asrar, G., & Nemani, R. R. (1997). Increased plant growth in the northern high latitudes from 1981 to 1991. *Nature*, *386*(6626), 698–702. https://doi.org/10.1038/386698a0

Nagai, S., Nasahara, K. N., Muraoka, H., Akiyama, T., & Tsuchida, S. (2010). Field experiments to test the use of the normalized-difference vegetation index for phenology detection. *Agricultural and Forest Meteorology*, *150*(2), 152–160. https://doi.org/10.1016/j.agrformet.2009.09.010

Nezval, O., Krejza, J., Světlík, J., Šigut, L., & Horáček, P. (2020). Comparison of traditional ground-based observations and digital remote sensing of phenological transitions in a floodplain forest. *Agricultural and Forest Meteorology*, *291*, 108079. https://doi.org/10.1016/j.agrformet.2020.108079

Pastorello, G. Z., Papale, D., Chu, H., Trotta, C., Agarwal, D. A., Canfora, E., Baldocchi, D., & Torn, M. S. (2017). A new data set to keep a sharper eye on land-air exchanges. *Eos, Transactions American Geophysical Union (Online)*. https://doi.org/10.1029/2017EO071597

Pau, S., Wolkovich, E. M., Cook, B. I., Davies, T. J., Kraft, N. J. B., Bolmgren, K., Betancourt, J. L., & Cleland, E. E. (2011). Predicting phenology by integrating ecology, evolution and climate science. *Global Change Biology*, *17*(12), 3633–3643. https://doi.org/10.1111/j.1365-2486.2011.02515.x

Paus, E., Nilsen, J., & Junttila, O. (1986). Bud dormancy and vegetative growth in salix-polaris as affected by temperature and photoperiod. *Polar Biology*, *6*(2), 91–95.

Peñuelas, J., Rutishauser, T., & Filella, I. (2009). Phenology feedbacks on climate change. *Science*, *324*(5929), 887–888. https://doi.org/10.1126/science.1173004

Piao, S., Ciais, P., Friedlingstein, P., Peylin, P., Reichstein, M., Luyssaert, S., Margolis, H., Fang, J., Barr, A., Chen, A., Grelle, A., Hollinger, D. Y., Laurila, T., Lindroth, A., Richardson, A. D., & Vesala, T. (2008). Net carbon dioxide losses of northern ecosystems in response to autumn warming. *Nature*, *451*(7174), 49–52. https://doi.org/10.1038/nature06444

Ren, J., Campbell, J., & Shao, Y. (2017). Estimation of SOS and EOS for midwestern US corn and soybean crops. *Remote Sensing*, *9*(7), 722. https://doi.org/10.3390/rs9070722

Rennenberg, H., Wildhagen, H., & Ehlting, B. (2010). Nitrogen nutrition of poplar trees. *Plant Biology*, *12*(2), 275–291. https://doi.org/10.1111/j.1438-8677.2009.00309.x

Richardson, A. D., Hufkens, K., Milliman, T., & Frolking, S. (2018). Intercomparison of phenological transition dates derived from the PhenoCam Dataset V1.0 and MODIS satellite remote sensing. *Scientific Reports*, *8*, 5679.

Richardson, A. D., Keenan, T. F., Migliavacca, M., Ryu, Y., Sonnentag, O., & Toomey, M. (2013). Climate change, phenology, and phenological control of vegetation feedbacks to the climate system. *Agricultural and Forest Meteorology*, *169*, 156–173. https://doi.org/10.1016/j.agrformet.2012.09.012

Saikkonen, K., Taulavuori, K., Hyvönen, T., Gundel, P. E., Hamilton, C. E., Vänninen, I., Nissinen, A., & Helander, M. (2012). Climate change-driven species' range shifts filtered by photoperiodism. *Nature Climate Change*, *2*(4), 239–242. https://doi.org/10.1038/nclimate1430

Sakai, A., & Larcher, W. (1987). *Frost survival of plants* (Vol. *62*). Springer Berlin Heidelberg.

Sen, P. K. (1968). Estimates of the regression coefficient based on Kendall's Tau. *Journal of the American Statistical Association*, *63*(324), 1379–1389. https://doi.org/10.1080/01621459.1968.10480934

Seyednasrollah, B., Young, A. M., Hufkens, K., Milliman, T., Friedl, M. A., Frolking, S., & Richardson, A. D. (2019). Tracking vegetation phenology across diverse biomes using Version 2.0 of the PhenoCam Dataset. *Scientific Data*, *6*(1), 222. https://doi.org/10.1038/s41597-019-0229-9

Seyednasrollah, B., Young, A. M., Hufkens, K., Milliman, T., Friedl, M. A., Frolking, S., Richardson, A. D., Abraha, M., Allen, D. W., Apple, M., Arain, M. A., Baker, J., Baker, J. M., Baldocchi, D., Bernacchi, C. J., Bhattacharjee, J., Blanken, P., Bosch, D. D., Boughton, R., … Zona, D. (2019). *PhenoCam dataset v2.0: Vegetation phenology from digital camera imagery, 2000–2018*. ORNL Distributed Active Archive Center.

Shang, R., Liu, R., Xu, M., Liu, Y., Zuo, L., & Ge, Q. (2017). The relationship between threshold-based and inflexion-based approaches for extraction of land surface phenology. *Remote Sensing of Environment*, *199*, 167–170. https://doi.org/10.1016/j.rse.2017.07.020

Shen, M., Jiang, N., Peng, D., Rao, Y., Huang, Y., Fu, Y. H., Yang, W., Zhu, X., Cao, R., Chen, X., Chen, J., Miao, C., Wu, C., Wang, T., Liang, E., & Tang, Y. (2020). Can changes in autumn phenology facilitate earlier green-up date of northern vegetation? *Agricultural and Forest Meteorology*, *291*, 108077. https://doi.org/10.1016/j.agrformet.2020.108077

Shen, M., Tang, Y., Desai, A. R., Gough, C., & Chen, J. (2014). Can EVI-derived land-surface phenology be used as a surrogate for phenology of canopy photosynthesis? *International Journal of Remote Sensing*, *35*(3), 1162–1174. https://doi.org/10.1080/01431161.2013.875636

Shen, M., Zhang, G., Cong, N., Wang, S., Kong, W., & Piao, S. (2014). Increasing altitudinal gradient of spring vegetation phenology during the last decade on the Qinghai–Tibetan Plateau. *Agricultural and Forest Meteorology*, *189-190*, 71–80. https://doi.org/10.1016/j.agrformet.2014.01.003

Shen, M. G., Piao, S. L., Jeong, S. J., Zhou, L. M., Zeng, Z. Z., Ciais, P., Chen, D., Huang, M., Jin, C.-S., Li, L. Z. X., Li, Y., Myneni, R. B., Yang, K., Zhang, G., Zhang, Y., & Yao, T. D. (2015). Evaporative cooling over the Tibetan Plateau induced by vegetation growth. *Proceedings of the National Academy of Sciences of the United States of America*, *112*(30), 9299–9304. https://doi.org/10.1073/pnas.1504418112

Soudani, K., Delpierre, N., Berveiller, D., Hmimina, G., & Dufrêne, R. (2021). A survey of proximal methods for monitoring leaf phenology in temperate deciduous forests. *Biogeosciences*, *18*(11), 3391–3408.

Soudani, K., Hmimina, G., Delpierre, N., Pontailler, J. Y., Aubinet, M., Bonal, D., Caquet, B., de Grandcourt, A., Burban, B., Flechard, C., Guyon, D., Granier, A., Gross, P., Heinesh, B., Longdoz, B., Loustau, D., Moureaux, C., Ourcival, J.-M., Rambal, S., … Dufrêne, E. (2012). Ground-based network of NDVI measurements for tracking temporal dynamics of canopy structure and vegetation phenology in different biomes. *Remote Sensing of Environment*, *123*, 234–245. https://doi.org/10.1016/j.rse.2012.03.012

Stinziano, J. R., & Way, D. A. (2017). Autumn photosynthetic decline and growth cessation in seedlings of white spruce are decoupled under warming and photoperiod manipulations. *Plant, Cell & Environment*, *40*(8), 1296–1316. https://doi.org/10.1111/pce.12917

Tang, J., Körner, C., Muraoka, H., Piao, S., Shen, M., Thackeray, S. J., & Yang, X. (2016). Emerging opportunities and challenges in phenology: A review. *Ecosphere*, *7*(8), e01436.

Taschler, D., & Neuner, G. (2004). Summer frost resistance and freezing patterns measured in situ in leaves of major alpine plant growth forms in relation to their upper distribution boundary. *Plant, Cell and Environment*, *27*(6), 737–746. https://doi.org/10.1111/j.1365-3040.2004.01176.x

Theil, H. (1992). A rank-invariant method of linear and polynomial regression analysis. In B. Raj & J. Koerts (Eds.), *Henri Theil's contributions to economics and econometrics: Econometric theory and methodology* (Vol. *23*, pp. 345–381). Springer Netherlands.

Thomas, H., & Stoddart, J. L. (1980). Leaf senescence. *Annual Review of Plant Physiology and Plant Molecular Biology*, *31*, 83–111. https://doi.org/10.1146/annurev.pp.31.060180.000503

Vermote, E. F. (2015). MOD09CMG MODIS/Terra surface reflectance daily L3 Global 0.05Deg CMG V006 [Data set]. *NASA EOSDIS Land Processes DAAC*. https://doi.org/10.5067/MODIS/MOD09CMG.006

Viovy, N. (2018). CRUNCEP Version 7 - atmospheric forcing data for the community land model [Data set]. In *Research Data Archive at the National Center for Atmospheric Research*. Computational and Information Systems Laboratory. https://doi.org/10.5067/MODIS/MOD09CMG.006

White, M. A., Thornton, P. E., & Running, S. W. (1997). A continental phenology model for monitoring vegetation responses to interannual climatic variability. *Global Biogeochemical Cycles*, *11*(2), 217–234. https://doi.org/10.1029/97gb00330

Wingate, L., Ogée, J., Cremonese, E., Filippa, G., Mizunuma, T., Migliavacca, M., Wilkinson, M., Moureaux, C., Wohlfahrt, G., Hammerle, A., Hörtnagl, L., Gimeno, C., Porcar-Castell, A., Galvagno, M., Nakaji, T., Morison, J., Kolle, O., Knohl, A., Kutsch, W., … Grace, J. (2015). Interpreting canopy development and physiology using a European phenology camera network at flux sites. *Biogeosciences*, *12*(20), 5995–6015. https://doi.org/10.5194/bg-12-5995-2015

Wu, C., Wang, X., Wang, H., Ciais, P., Peñuelas, J., Myneni, R. B., Desai, A. R., Gough, C. M., Gonsamo, A., Black, A. T., Jassal, R. S., Ju, W., Yuan, W., Fu, Y., Shen, M., Li, S., Liu, R., Chen, J. M., & Ge, Q. (2018). Contrasting responses of autumn-leaf senescence to daytime and night-time warming. *Nature Climate Change*, *8*(12), 1092–1096. https://doi.org/10.1038/s41558-018-0346-z

Xu, C., Liu, H., Williams, A. P., Yin, Y., & Wu, X. (2016). Trends toward an earlier peak of the growing season in Northern Hemisphere mid-latitudes. *Global Change Biology*, *22*(8), 2852–2860. https://doi.org/10.1111/gcb.13224

Yang, X., Tang, J., & Mustard, J. F. (2014). Beyond leaf color: Comparing camera-based phenological metrics with leaf biochemical, biophysical, and spectral properties throughout the growing season of a temperate deciduous forest. *Journal of Geophysical Research: Biogeosciences*, *119*(3), 181–191. https://doi.org/10.1002/2013jg002460

Ye, Y., & Zhang, X. (2021). Exploration of global spatiotemporal changes of fall foliage coloration in deciduous forests and shrubs using the VIIRS land surface phenology product. *Science of Remote Sensing*, *4*, 100030. https://doi.org/10.1016/j.srs.2021.100030

Yu, H., Luedeling, E., & Xu, J. (2010). Winter and spring warming result in delayed spring phenology on the Tibetan Plateau. *Proceedings of the National Academy of Sciences of the United States of America*, *107*(51), 22151–22156. https://doi.org/10.1073/pnas.1012490107

Zhang, X. (2015). Reconstruction of a complete global time series of daily vegetation index trajectory from long-term AVHRR data. *Remote Sensing of Environment*, *156*, 457–472. https://doi.org/10.1016/j.rse.2014.10.012

Zhang, X., Friedl, M. A., Schaaf, C. B., Strahler, A. H., Hodges, J. C., Gao, F., Reed, B. C., & Huete, A. (2003). Monitoring vegetation phenology using MODIS. *Remote Sensing of Environment*, *84*(3), 471–475.

Zhang, X., Tarpley, D., & Sullivan, J. T. (2007). Diverse responses of vegetation phenology to a warming climate. *Geophysical Research Letters*, *34*(19), L194. https://doi.org/10.1029/2007gl031447

Zhao, B., Donnelly, A., & Schwartz, M. D. (2020). Evaluating autumn phenology derived from field observations, satellite data, and carbon flux measurements in a northern mixed forest, USA. *International Journal of Biometeorology*, *64*(5), 713–727. https://doi.org/10.1007/s00484-020-01861-9

Zohner, C. M., Benito, B. M., Svenning, J.-C., & Renner, S. S. (2016). Day length unlikely to constrain climate-driven shifts in leaf-out times of northern woody plants. *Nature Climate Change*, *6*(12), 1120–1123. https://doi.org/10.1038/nclimate3138

BIOSKETCH

Miaogen Shen is a professor at the Beijing Normal University, China. He is interested in interactions between vegetation and climate. More information is available at: https://www.researchgate.net/profile/Miaogen-Shen.

SUPPORTING INFORMATION

Additional supporting information can be found online in the Supporting Information section at the end of this article.

How to cite this article: Jiang, N., Shen, M., Ciais, P., Campioli, M., Peñuelas, J., Körner, C., Cao, R., Piao, S., Liu, L., Wang, S., Liang, E., Delpierre, N., Soudani, K., Rao, Y., Montagnani, L., Hörtnagl, L., Paul-Limoges, E., Myneni, R., Wohlfahrt, G. … Zhao, W. (2022). Warming does not delay the start of autumnal leaf coloration but slows its progress rate. *Global Ecology and Biogeography*, *31*, 2297–2313. https://doi.org/10.1111/geb.13581